Elementary Reaction Mechanism for Benzene Oxidation in Supercritical Water†

Joanna L. DiNaro,‡ Jack B. Howard,§ William H. Green,|| Jefferson W. Tester,*,‡ and Joseph W. Bozzelli⊥

Department of Chemical Engineering and Energy Laboratory, Massachusetts Institute of Technology, 77 Massachusetts Avenue, Cambridge, Massachusetts 02139, and Chemistry and Chemical Engineering Department, New Jersey Institute of Technology, Newark, New Jersey

Received: April 13, 2000; In Final Form: August 31, 2000

Supercritical water (SCW) benzene oxidation data were modeled using a published, low-pressure (<1 bar) benzene combustion mechanism and submechanisms describing the oxidation of key intermediate species. To adapt the low-pressure, gas-phase benzene combustion mechanism to the lower temperature (<700 °C or 975 K) and higher pressure (>220 bar) conditions, new reaction pathways were added, and quantum Rice−Ramsperger−Kassel theory was used to calculate the rate coefficients and, hence, product selectivities for pressure dependent reactions. The most important difference between the benzene oxidation mechanism for SCW conditions and those for combustion conditions is reactions in SCW involving C_6H_5OO predicted to be formed by C_6H_5 reacting with O_2. Through the adjustment of the rate coefficients of two thermal decomposition pathways of C_6H_5OO, whose values are unknown, the model accurately predicts the measured benzene and phenol concentration profiles at 813 K (540 °C), 246 bar, stoichiometric oxygen, and 3−7 s residence time. Comparison of the model predictions to benzene SCW oxidation data measured at several different conditions reveals that the model qualitatively explains the trends of the data and gives good quantitative agreement with no further adjustment of the rate coefficients. For example, the model predicts the benzene reaction to within ±10% conversion at temperatures between 790 and 860 K (515 and 590 °C) at 246 bar with stoichiometric oxygen and at pressures from 139 to 278 bar at 813 K (540 °C) with stoichiometric oxygen.

Introduction and Background

Supercritical water oxidation (SCWO) is a remediation process for treating aqueous organic wastes. The process usually operates between 775 and 900 K and from 250 to 280 bar. When organic compounds and oxygen are brought together in water well above its critical point of 221 bar and 374 °C (647 K), organics are oxidized to carbon dioxide and water; heteroatoms such as chlorine, sulfur, and phosphorus are converted to their corresponding mineral acids and can be neutralized using a suitable base; and any nitrogen forms N_2 or N_2O.[1] NO_x gases, typical undesired byproducts of combustion processes, are not formed because these oxidation pathways are not favored at the lower temperatures of SCWO. Reviews of the SCWO process can be found in Modell,[2] Tester et al.,[3] Gloyna and Li,[4] and Tester and Cline.[5]

The present working hypothesis maintains that SCWO proceeds by free-radical reactions and that the individual elementary reactions are similar to those which would take place in combustion at the temperature and pressure of SCWO. Furthermore, water, which serves as the reaction medium and participates in reactions both as a reactant and as a third-body collider, does not interfere with reaction events through solvation effects. This hypothesis is derived from the evidence that water above its critical point closely resembles a nonpolar, dense gas.[6−9] At typical commercial SCWO conditions, water densities range from 0.07 to 0.1 g/mL and the viscosity is about a factor of 25 lower than at ambient conditions.[10] The static dielectric constant of water at 250 bar decreases from its room temperature value of 78 to a value of 1−2 at 775 K.[11] As a consequence the ion product of water, K_w, at 250 bar decreases with increasing temperature in the range of 725−875 K from its subcritical value of approximately 10^{-14} to 10^{-23}, indicating that water only weakly dissociates and poorly solvates ions in its supercritical state.[12] Since supercritical water cannot support charged species in the fully supercritical region, free-radical reactions are assumed to dominate over ionic reactions.

The free-radical reaction pathway hypothesis has received support by multiple attempts to model oxidation in SCW using low-pressure combustion mechanisms adapted to SCWO conditions. Previous modeling efforts yielded kinetic mechanisms describing the oxidation of simple compounds such as hydrogen,[6−8,13−15] carbon monoxide,[7,8,13] methane,[7,8,16,17] methanol,[8,9,15,18−21] and phenol.[22] The model predictions have been compared, with varying degrees of success, to experimentally measured species concentration profiles.

In related documentation,[23] we report experimental results on benzene SCWO at 750−860 K and sub- to supercritical pressures (139−278 bar) under fuel-rich to fuel-lean conditions. The concentration profiles of benzene, phenol, carbon monoxide, carbon dioxide, and methane were measured as a function of reactor residence times of 3−7 s. In the present paper, a low-pressure, gas-phase benzene combustion mechanism is used to model these experimental data. A discussion of the primary

† Part of the special issue "C. Bradley Moore Festschrift".

* To whom correspondence should be addressed. Telephone: (617) 253−3401. Fax: (617) 253−8013. E-mail: testerel@mit.edu.

‡ Department of Chemical Engineering and Energy Laboratory, Massachusetts Institute of Technology, Rm E40-455.

§ Department of Chemical Engineering, Massachusetts Institute of Technology, Rm 66-445. Telephone: (617) 253-4574. Fax: (617) 258-5042. E-mail: jbhoward@mit.edu.

|| Department of Chemical Engineering, Massachusetts Institute of Technology, Rm 66-448. Telephone: (617) 253−4580. Fax: (617) 253−1651. E-mail: whgreen@mit.edu.

⊥ Chemistry and Chemical Engineering Department, New Jersey Institute of Technology. E-mail: bozzelli@njit.edu.

10.1021/jp001390e CCC: $19.00
Published on Web 10/25/2000

differences between this low-pressure combustion mechanism and that developed here for SCWO conditions can be found in DiNaro et al.[24]

Several mechanisms have been developed to model benzene combustion at ambient to subambient pressures. The review article by Brezinsky[25] presented a qualitative mechanism for benzene oxidation. Bittker[26] expanded on that mechanism and successfully predicted the trends and found good quantitative agreement with several of the composition profiles of Lovell et al.[27] and the ignition delay times of Burcat et al.[28] Emdee et al.[29] developed a mechanism for describing the oxidation of toluene to benzene near 1200 K. The model contained a 68 reaction benzene submechanism. Linstedt and Skevis[30] developed a 395 reaction benzene oxidation mechanism with many reactions and rate coefficients taken from the benzene submechanism in the Emdee et al. model. They validated their model against the premixed benzene−oxygen−argon flame data of Bittner and Howard[31] measured at 20 Torr and under fuel-rich, "near-sooting" conditions with a temperature profile which ranged from ambient to 1900 K. Excellent agreement was obtained with the experimental profiles for benzene, carbon monoxide, carbon dioxide, oxygen, and other radical and stable species, but phenoxy (C_6H_5O), phenyl (C_6H_5), and phenol (C_6H_5-OH) were all overpredicted. Zhang and McKinnon[32] also used the Emdee et al. benzene submechanism as a starting point and developed a 514 elementary reaction mechanism for benzene oxidation which they, too, tested against the data of Bittner and Howard.[31] Most of the rate coefficients were taken from the literature, but some—most notably those involving cyclopentadienyl (C_5H_5) —had to be estimated. Some elementary reactions were taken from Bittker's[26] model. Since the Bittner and Howard[31] data were measured at 20 Torr, Zhang and McKinnon accounted for the pressure dependence of unimolecular (falloff) and bimolecular (chemical activation) reactions using the quantum Rice−Ramsperger−Kassel, QRRK, method.[33] Their resulting pressure-corrected mechanism gave good quantitative agreement for benzene and many other stable and radical intermediate species. Like the Lindstedt−Skevis mechanism, however, their model overpredicted both C_6H_5 and C_6H_5O.

Using net rate analysis, Shandross[34,35] evaluated the ability of the Lindstedt−Skevis (LS), Zhang−McKinnon (ZM), and Emdee−Brezinsky−Glassman (EBG) models to predict his experimental profiles of 44 species in a fuel-rich, 22 Torr, laminar, premixed hydrogen−oxygen−argon flame seeded with benzene at temperatures up to 1940 K. He found that the three mechanisms strongly overpredicted phenol destruction at high temperatures. Using the ZM mechanism as a basis, Shandross modified reactions of benzene and phenol, used bimolecular QRRK and Rice−Ramsperger−Kassel−Marcus (RRKM)[33] methods to account for the pressure dependence of rate coefficients, and added new reactions. The modified mechanism gave improved agreement with the C_6H_5OH chemistry, but the destruction rate was still overpredicted. The net rates of the other critical intermediates, C_6H_5, C_6H_5O, and C_6H_5OH, also were not well predicted.

Tan and Frank[36] developed a benzene oxidation mechanism built on an earlier model for combustion of methane to propane and their mixtures.[37] Reactions involving C_5 and C_6 were added with updated rate coefficients. The model relies heavily on the shock tube investigation of reactions between phenyl and oxygen by Frank et al.[38] New reaction pathways leading to the formation of *p*-benzoquinone ($C_6H_4O_2$) and its subsequent reaction were included. Excellent agreement between model predictions and experimental data was obtained for benzene, carbon monoxide, carbon dioxide, and other stable and radical species. Uncertainty was still present in the reactions involving C_5 species, and, as with the other benzene mechanisms, C_6H_5 was overpredicted, although by a lesser amount than in previous modeling attempts.

Here, the low-pressure, gas-phase benzene combustion mechanism of Shandross[34,35] is adapted to SCW conditions and used to model our experimentally measured benzene SCWO data. QRRK was used to calculate pressure dependent rate coefficients, and new reaction pathways were included in order to explain the experimental data. There are two reasons for the current study: (1) to gain mechanistic insight into the oxidation of benzene in supercritical water and (2) to determine if existing free-radical reaction network models of benzene oxidation at atmospheric, combustion conditions can describe benzene oxidation in SCW.

The combustion mechanisms reviewed above successfully predict the oxidation of benzene as well as many other stable and radical intermediates. The main shortcomings of these models are their overpredictions of C_6H_5, C_6H_5O, and C_6H_5-OH. This inaccuracy is troubling since these species are the primary products of benzene oxidation. As noted by Chai and Pfefferle,[39] the current benzene oxidation models, developed primarily for temperatures above 1600 K and fuel-rich conditions, are not useable outside of the temperature and stoichiometric conditions for which they were adjusted, and the understanding of the detailed oxidation mechanism is particularly poor at 900−1300 K and fuel-lean conditions.

Applying a low-pressure benzene combustion mechanism to SCW conditions may further the understanding of benzene combustion. Since the SCWO data are measured at lower temperatures (750−860 K) and much higher pressures (139−278 bar) than those for which the mechanisms were originally developed, the dominant oxidation pathways may differ. For example, thermal decomposition pathways with high activation barriers, which play important roles at combustion conditions, may be inaccessible. Therefore, comparisons of the predictions of a current benzene combustion mechanism[34,35] against SCWO data will test the robustness of the mechanism and could further the understanding of the benzene oxidation mechanism.

Adaptation to Supercritical Water Conditions

The mechanism of Shandross[34,35] was reduced to 41 reactions using an automatic sensitivity coefficient guided model reduction algorithm:[40] an efficient, automated method for model reduction whereby individual reactions are removed on the basis of their sensitivity coefficients followed by simulation of the model to ensure that predicted concentrations do not change outside of a predetermined tolerance. Figure 1 compares concentration profiles of C_6H_6 and C_6H_5OH calculated by SENKIN[41] using this reduced mechanism and the thermochemistry from Table 1 with data measured at 813 K and 246 bar with stoichiometric oxygen. The model overpredicts the oxidation rate of benzene and the concentration of phenol.

To improve the agreement between the model and the experimental data, the reactions and rate coefficients in the reduced mechanism were evaluated and updated where necessary. The final reduced model is shown in Table 2. The rate coefficient for R11, the abstraction of H from C_6H_6 by OH, was updated to the recommended value of Baulch et al.,[42] which is not significantly different from the value used by Shandross.[43] The abstraction of the phenolic H from phenol by O (R17) was updated to the value recommended by Baulch et al.[44] and used by Tan and Frank.[36] At 813 K this rate coefficient is an order of magnitude larger than that used by Shandross.[29] The thermal

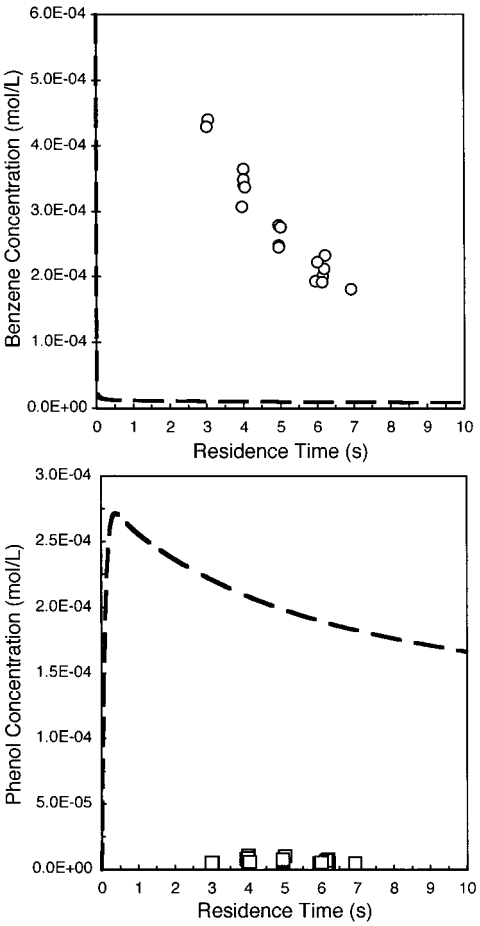

Figure 1. Comparison of experimental data (open symbols) and predicted benzene and phenol concentrations (dashed lines) using the mechanism of Shandross: $T = 813$ K; $P = 246$ bar; $\Phi = 1.0$; $[C_6H_6]_0 = 0.6 \times 10^{-3}$ mol/L.

decomposition of phenoxy (R23) was updated from the value used in the ZM model to reflect the recently reported value of Frank et al.[38]

The rate coefficients of unimolecular and pressure dependent, chemically activated bimolecular reactions were calculated for a pressure of 246 bar and temperatures between 300 and 1000 K using the QRRK analysis of Dean[45] as implemented by CHEMACT[46] and CHEMDIS.[47,48] A detailed discussion of the governing bimolecular and unimolecular QRRK equations is given in Westmoreland et al.[49] and Dean.[45]

The input data necessary for performing the QRRK calculations can be found in Tables IS−VS, but brief descriptions of the reactions evaluated by this method follow. The reaction between H and O_2 to form OH and O is one of the most important chain-branching steps in low-pressure combustion. The addition/elimination pathway proceeds through the formation of the activated intermediate HO_2^* which can be stabilized to HO_2 (R1) or dissociate to OH and O (R6). The relative importance of the two pathways depends on pressure and temperature with the HO_2-forming pathway favored at higher pressures. At 246 bar and 813 K, the reaction between H and O_2 primarily forms the stabilization product HO_2 with a rate constant close to the high-pressure limit (k_∞) reported by Cobos et al.[50] (see Table IS). The dissociation of H_2O_2 to $(OH)_2$ was estimated using data for k_∞ reported by Fulle et al.[51] (see Table IIS). The rate coefficient for R5 ($OH + HO_2 \leftrightarrow H_2O + O_2$) was updated to the value used in a moist CO oxidation mechanism developed for pressures from 1 to 9.7 bar and temperatures from 960 to 1200 K.[53] The rate coefficient for R81 ($C_2H_3 \leftrightarrow C_2H_2 + H$) was calculated using k_∞ recommended by Warnatz[54] (see Table IIIS). The resulting predicted rate coefficient at 246 bar is close to the high-pressure limit. The reaction of CO and O to form CO_2 (R84) was found to be in its high-pressure limit at 246 bar (see Table IVS), and the k_∞ reported by Troe[55] is used here.

The identity and formation rate of products of the reaction between phenyl (C_6H_5) and oxygen (O_2) are a focus of continuing study. Yu and Lin[56] performed a direct study on the reaction between C_6H_5 and O_2 at 297−500 K and 20−80 Torr and found that the reaction proceeds through the formation of an energized phenylperoxy radical ($C_6H_5OO^*$). $C_6H_5OO^*$ then undergoes stabilization, isomerization, and/or dissociation to new products. The dominant pathway depends on the temperature and pressure. In the Yu and Lin study, the sole reaction product was C_6H_5OO.

In most previous benzene mechanisms,[26,29,30] the products of this reaction have been set to phenoxy (C_6H_5O) and O with a rate coefficient independent of pressure. Shandross[34,35] calculated the rate coefficient for the pathway to C_6H_5O and O to account for the effects of temperature and pressure. A semiglobal pathway to CO, C_2H_2 and C_2H_3 has been included in some mechanisms.[31,33,34]

Frank et al.[38] studied the reaction of C_6H_5 with O_2 between 900 and 1800 K and from 1.3 to 2.5 bar and proposed two sets of products: C_6H_5O and O; and *p*-benzoquinone ($C_6H_4O_2$) and H. The second of these addition/elimination pathways was necessary to explain their observation of fast initial H production. Rate coefficients were measured for both pathways and included in a mechanism by Tan and Frank.[36]

Since the reaction of C_6H_5 and O_2 proceeds through the formation of $C_6H_5OO^*$, the rate coefficients for the addition/elimination pathways measured by Frank et al.[38] or used in low-pressure mechanisms[26,29,30,32,34−36] are not applicable at SCWO conditions. CHEMDIS was used to calculate the rate coefficients for stabilization to C_6H_5OO and addition/elimination to C_6H_5O and O (see Table VS). The high-pressure rate coefficient for C_6H_5OO formation was taken from Yu and Lin,[56] and the high-pressure rate coefficient for dissociation of $C_6H_5OO^*$ to C_6H_5O and O was estimated from microscopic reversibility and assuming the reverse reaction has a preexponential factor for diffusion controlled reactions ($A = 10^{12}$ cm^3 mol^{-1} s^{-1}) and no energy barrier ($E_a = 0$). At 813 K and 246 bar, the calculated stabilization rate coefficient is 2 orders of magnitude larger than that for addition/elimination to C_6H_5O and O. A comparison between the predicted and measured[38] rate coefficients for the addition/elimination pathway at 2.3 bar and from 1000 to 1200 K showed agreement to within 10−20%, indicating that the estimated value of k_∞ for $C_6H_5OO^*$ dissociation to C_6H_5O and O may not be a source of significant error.

Since C_6H_5OO was predicted to be the main reaction product of C_6H_5 and O_2, bimolecular (R28−R31) and unimolecular (R27, *R*32, and R33) reactions of C_6H_5OO were included in the SCW benzene oxidation mechanism. The rate coefficients of the bimolecular reactions were estimated as explained in the footnotes of Table 2. The rate coefficient for R27

$$C_6H_5OO \leftrightarrow C_6H_5O + O \qquad \text{(R27)}$$

was calculated in the QRRK analysis. The rate coefficient for R32

$$C_6H_5OO \leftrightarrow C_6H_4O_2 + H \qquad \text{(R32)}$$

TABLE 1: Thermodynamic Data Used in the SCW Benzene Oxidation Mechanism

	kcal/mol	cal/(mol K)								
species	$\Delta H_f(298)$	$S(298)$	$C_P(300)$	$C_P(400)$	$C_P(500)$	$C_P(600)$	$C_P(800)$	$C_P(1000)$	$C_P(1500)$	source[a]
C_7H_7	47.80	75.58	25.45	33.50	40.38	46.07	54.30	60.02	67.99	70
C_7H_8	11.95	76.46	24.88	33.30	40.62	46.78	55.95	62.35	71.37	70
C_6H_6	19.81	64.37	19.92	27.09	33.25	38.38	45.87	51.05	58.31	
C_6H_5	79.44	69.83	21.01	27.06	32.43	37.05	43.90	47.77	53.26	68
C_6H_5O	10.36	74.89	24.79	31.31	37.08	42.01	49.25	53.28	58.98	68
C_6H_5OH	−23.06	75.39	24.86	32.53	38.71	43.65	50.76	55.62	62.81	71
$C_6H_4O_2$	−29.37	79.62	26.04	32.20	37.67	42.27	48.87	53.42	59.48	*b*
C_6H_5OO	37.04	85.62	26.76	34.25	40.07	44.82	51.76	56.48		68
C_6H_5OOH	0.94	85.40	28.81	37.09	43.62	48.91	56.48	61.45		68
C_5H_5O	42.94	72.73	20.60	27.20	32.60	36.99	43.44	47.73	54.07	60
C_5H_4OH	16.88	75.23	21.69	28.61	34.08	38.38	44.34	48.04	53.24	60
C_5H_6	31.26	65.50	18.23	24.76	30.15	34.59	41.25	45.81	52.50	60
C_5H_4	111.07	70.89	20.93	25.14	28.52	31.23	35.29	38.35	42.92	*b*
C_5H_4O	7.40	66.71	19.50	25.73	30.87	34.78	40.31	44.27	49.40	60
C_5H_5	57.17	63.58	17.86	24.30	29.47	33.58	39.46	43.26	48.68	60
C_5H_3	135.42	70.54	21.05	24.28	27.00	29.23	32.47	34.91	38.45	
$C_5H_5O_{1-2}$	23.14	75.73	20.84	27.24	32.35	36.29	42.39	46.69		59
C_4H_6	34.97	68.17	18.80	22.74	26.39	29.69	35.17	39.30	45.45	
C_4H_4	73.63	66.65	17.57	21.18	24.19	26.68	30.49	33.17	37.33	
CH_2CHCCH_2	74.11	69.81	19.69	23.74	27.10	29.88	34.09	37.04	41.67	
$CH_2CHCHCH$	83.99	69.05	19.06	23.57	27.22	30.15	34.45	37.38	42.05	60
H_2CCCCH	111.33	72.96	20.24	22.43	24.44	26.23	29.10	30.93	33.68	
C═CCC═COH	7.18	85.00	25.04	32.22	38.11	42.79	49.59	54.34	61.52	59
COC═CKET	−31.02	84.13	28.43	34.43	39.29	42.26	46.62	49.94	54.31	60
C═CC═C═O	1.82	71.96	21.62	26.23	30.23	32.64	36.20	39.20	43.21	60
H_2CCCH	83.05	61.49	15.84	17.74	19.47	21.01	23.43	25.00	27.55	
C_3H_6	4.89	61.52	15.46	19.27	22.73	25.80	30.78	34.52	40.14	
C_3H_5	40.75	63.02	14.96	18.61	21.75	24.43	28.67	31.74	36.33	60
C_2H_2	54.20	48.02	10.62	11.99	13.08	13.95	15.27	16.31	18.27	
C_2H_3	68.42	55.33	9.57	11.19	12.78	14.31	16.98	18.75	21.26	
C_2H_4	12.54	52.38	10.23	12.79	14.94	16.83	20.05	22.51	26.22	
CH_4	−17.90	44.47	8.43	9.84	11.14	12.41	15.00	17.25	20.63	
HCO	10.40	53.66	8.24	8.78	9.28	9.77	10.74	11.52	12.56	
CH_3	34.82	46.38	9.23	10.09	10.83	11.52	12.87	14.12	16.27	
CH_2O	−27.70	52.25	8.40	9.50	10.50	11.47	13.36	14.88	16.97	
CH_2	101.51	45.10	8.07	8.30	8.60	8.98	9.85	10.61	11.83	
CO	−26.42	47.21	6.95	7.03	7.14	7.27	7.61	7.95	8.41	
CO_2	−94.06	51.08	8.91	9.86	10.65	11.31	12.32	12.99	13.93	
H_2O	−57.80	45.10	8.00	8.23	8.44	8.67	9.22	9.87	11.26	
H_2O_2	−32.53	55.66	10.41	11.44	12.34	13.11	14.29	15.21	16.85	
H_2	.00	31.21	6.90	6.96	7.00	7.02	7.07	7.21	7.73	
O	59.56	38.47	5.23	5.14	5.08	5.05	5.02	5.00	4.98	
HO_2	3.00	54.73	8.34	8.95	9.49	9.97	10.78	11.39	12.45	
O_2	.00	49.01	7.01	7.22	7.44	7.65	8.07	8.35	8.72	
OH	9.32	43.88	7.15	7.10	7.07	7.06	7.13	7.33	7.87	
H	52.10	27.39	4.97	4.97	4.97	4.97	4.97	4.97	4.97	

[a] Taken from Kee et al.[72] unless otherwise noted. [b] Alzueta et al.[58] (taken from Burcat and McBride[73]).

was treated as an adjustable parameter in the present model. Another dissociation pathway of C_6H_5OO, which was proposed by Carpenter[57]

$$C_6H_5OO \leftrightarrow C_5H_5 + CO_2 \qquad \text{(R33)}$$

was also tested in the present model, again by treating the rate coefficient as an adjustable parameter. The effects of the inclusion of these two additional dissociation pathways will be discussed in detail in the analysis of the mechanism.

Two pathways leading to the formation of $C_6H_4O_2$ were included. The first

$$C_6H_5O + O \leftrightarrow C_6H_4O_2 + H \qquad \text{(R23)}$$

was proposed by Frank et al.[38] and used in the Tan and Frank benzene oxidation mechanism.[36] The second pathway

$$C_6H_5OO \leftrightarrow C_6H_4O_2 + H \qquad \text{(R32)}$$

is speculated to occur in the present work. Tan and Frank[36] assumed $C_6H_4O_2$ decomposed to C_5H_4O and CO, and C_5H_4O to C_4H_4 and CO at their conditions. Here, we include the recently developed submechanism for *p*-benzoquinone oxidation[58] to account for further reactions of $C_6H_4O_2$ (R34−R44, R46−R48, and R50−R53).

The reactions and associated rate coefficients of the reactions involving C_5H_5 and C_5H_6 in the Shandross mechanism were taken from the EBG mechanism.[29] Emdee et al. estimated the abstraction of H from C_5H_6 by HO_2, OH, H, and O from the analogous reactions with formaldehyde and based the C_5H_5 submechanism on the outline presented by Brezinsky.[25] Zhong and Bozzelli[59,60] recently assembled submodels of cyclopentadiene (C_5H_6) and cyclopentadienyl (C_5H_5) reactions with H, O, OH, HO_2, and O_2 for insertion in combustion mechanisms where these species are important. For the present mechanism, CHEMDIS was used to predict rate coefficients for the addition and combination reactions of C_5H_5 and C_5H_6 with H, O, OH, HO_2, and O_2 at 246 bar from 300 to 1000 K using the thermodynamic data, high-pressure rate coefficients, vibrational frequencies, and Lennard-Jones parameters presented in these

TABLE 2: Reduced Elementary Reaction Mechanism for Benzene Oxidation in SCW (Mechanism Developed for a Pressure of 246 bar and Temperatures around 813 K; the Rate Coefficient Used Is Identical to That Used by Shandross[34,35] If "Unchanged" Follows the Reference)

no.	reaction	A (cm^3 mol s)	n	E_a (cal/mol)	ref
		H_2/O_2 reactions			
1	$H + O_2 \leftrightarrow HO_2$	2.07×10^{18}	−1.69	890	QRRK
2	$O_2 + HO_2 \leftrightarrow H_2O_2 + O_2$	2.22×10^{11}	0.	−1 629	*a* (unchanged)
3	$H_2O_2 + OH \leftrightarrow H_2O + HO_2$	7.83×10^{12}	0.	1 331.4	42 (unchanged)
4	$OH + OH \leftrightarrow H_2O_2$	2.96×10^{28}	−5.26	2 980	QRRK
5	$OH + HO_2 \leftrightarrow H_2O + O_2$	1.91×10^{16}	−1.0	0	53
6	$H + O_2 \leftrightarrow OH + O$	2.10×10^{15}	−0.3	20 200	QRRK
7	$OH + OH \leftrightarrow O + H_2O$	1.50×10^{9}	1.14	99.4	42 (unchanged)
8	$O + HO_2 \leftrightarrow OH + O_2$	3.25×10^{13}	0.	0	42 (unchanged)
		C_7H_7 reactions			
9	$C_5H_5 + C_2H_2 \leftrightarrow C_7H_7$	3.72×10^{11}	0.	8 300	32 (unchanged)
10	$C_7H_8 + OH \leftrightarrow C_7H_7 + H_2O$	1.26×10^{13}	0.	2 583	29 (unchanged)
		C_6H_6 reactions			
11	$OH + C_6H_6 \leftrightarrow C_6H_5OH + H$	1.34×10^{13}	0.	10 592	69 (unchanged)
12	$OH + C_6H_6 \leftrightarrow C_6H_5 + H_2O$	1.63×10^{8}	1.42	1 454	42
13	$O + C_6H_6 \leftrightarrow C_6H_5O + H$	2.40×10^{13}	0.	4 668	74 (unchanged)
		C_6H_5OH reactions			
14	$H + C_6H_5O \leftrightarrow C_6H_5OH$	2.50×10^{14}	0.	0	69 (unchanged)
15	$OH + C_6H_5OH \leftrightarrow H_2O + C_6H_5O$	1.39×10^{8}	1.43	−962	34 (unchanged)
16	$C_6H_5OH + O \leftrightarrow C_6H_5O + OH$	1.28×10^{13}	0.	2 891	36, 44
17	$C_6H_5OH + HO_2 \leftrightarrow C_6H_5O + H_2O_2$	3.00×10^{13}	0.	15 000	26 (unchanged)
18	$C_6H_5OH + CH_2CHCHCH \leftrightarrow C_4H_6 + C_6H_5O$	6.00×10^{12}	0.	0	29 (unchanged)
19	$C_6H_5OH + CH_2CHCCH_2 \leftrightarrow C_4H_6 + C_6H_5O$	6.00×10^{12}	0.	0	29 (unchanged)
20	$C_6H_5OH + C_6H_5 \leftrightarrow C_6H_6 + C_6H_5O$	4.91×10^{12}	0.	4 400	29 (unchanged)
		C_6H_5O reactions			
21	$C_6H_5O + C_5H_6 \leftrightarrow C_5H_5 + C_6H_5OH$	3.16×10^{11}	0.	8 000	29 (unchanged)
22	$C_6H_5O \leftrightarrow C_5H_5 + CO$	7.40×10^{11}	0.	43 853	38
23	$C_6H_5O + O \leftrightarrow C_6H_4O_2 + H$	3.00×10^{13}	0.	0	36
		C_6H_5 reactions			
24	$C_6H_5 + O \leftrightarrow C_5H_5 + CO$	9.00×10^{13}	0.	0	38
25	$C_6H_5 + O_2 \leftrightarrow C_6H_5O + O$	2.57×10^{-29}	12.73	−5 699	QRRK
26	$C_6H_5 + O_2 \leftrightarrow C_6H_5OO$	1.85×10^{13}	−0.15	−159	QRRK
		C_6H_5OO reactions			
27	$C_6H_5OO \leftrightarrow C_6H_5O + O$	4.27×10^{15}	−0.7	33 027	QRRK
28	$C_6H_5OO + H \leftrightarrow C_6H_5OOH$	2.50×10^{14}	0.	0	*b*
29	$C_6H_5O + OH \leftrightarrow C_6H_5OOH$	1.00×10^{12}	0.	0	*c*
30	$C_6H_5OO + C_6H_5OH \leftrightarrow C_6H_5OOH + C_6H_5O$	$1.00 \times 10^{11.5}$	0.	6 961	*d*
31	$C_6H_5OO + HO_2 \leftrightarrow C_6H_5OOH + O_2$	1.87×10^{12}	0.	1 540	*e*
32	$C_6H_5OO \leftrightarrow C_6H_4O_2 + H$	4.00×10^{8}	0.	0	*f*
33	$C_6H_5OO \leftrightarrow C_5H_5 + CO_2$	1.60×10^{8}	0.	0	*f*
		$C_6H_4O_2$ reactions			
34	$C_6H_4O_2 \leftrightarrow C_5H_4O + CO$	3.70×10^{11}	0.	59 000	58
35	$C_6H_4O_2 \leftrightarrow C_5H_4 + CO_2$	3.50×10^{12}	0.	67 000	58
36	$C_6H_4O_2 + H \leftrightarrow C_5H_5O + CO$	2.50×10^{13}	0.	4 700	58
37	$C_6H_4O_2 + H \rightleftharpoons C_6H_3O_2 + H_2$	2.00×10^{12}	0.	8 100	58
38	$C_6H_4O_2 + OH \rightleftharpoons C_6H_3O_2 + H_2O$	1.00×10^{6}	2.0	4 000	58
39	$C_6H_4O_2 + O \rightleftharpoons C_6H_3O_3 + H$	1.50×10^{13}	0.	4 530	58
40	$C_6H_4O_2 + O \rightleftharpoons C_6H_3O_2 + OH$	1.40×10^{13}	0.	14 700	58
		$C_6H_3O_2$ reactions			
41	$C_6H_3O_2 + H \rightleftharpoons 2C_2H_2 + 2CO$	1.00×10^{14}	0.	0	58
42	$C_6H_3O_2 + O \rightleftharpoons C_2H_2 + HCCO + 2CO$	1.00×10^{14}	0.	0	58
43	$C_6H_3O_3 \rightleftharpoons C_2H_2 + HCCO + 2CO$	1.00×10^{12}	0.	50 000	58
		C_5H_5O reactions			
44	$C_5H_5O \leftrightarrow CH_2CHCHCH + CO$	7.50×10^{11}	0.	43 900	58
		C_5H_4O reactions			
45	$C_5H_4O \leftrightarrow C_4H_4 + CO$	1.00×10^{12}	0.	0	36
46	$C_5H_4O + O \rightleftharpoons C_4H_4 + CO_2$	1.00×10^{13}	0.	2 000	58
47	$C_5H_4O + H \leftrightarrow CH_2CHCCH_2 + CO$	2.50×10^{13}	0.	4 700	58
48	$C_5H_4O \leftrightarrow 2C_2H_2 + CO$	1.00×10^{15}	0.	78 000	58
59	$C_5H_4OH \leftrightarrow C_5H_4O + H$	2.13×10^{13}	0.	48 000	29
		C_5H_4 reactions			
50	$C_5H_4 + H \leftrightarrow C_5H_3 + H_2$	1.00×10^{6}	2.5	5 000	58
51	$C_5H_4 + O \leftrightarrow C_5H_3 + OH$	1.00×10^{6}	2.5	3 000	58
52	$C_5H_4 + OH \leftrightarrow C_5H_3 + H_2O$	1.00×10^{7}	2.0	0	58
		C_5H_3 reactions			
53	$C_5H_3 + O_2 \leftrightarrow C_2H_2 + HCCO + CO$	1.00×10^{12}	0.	0	58

TABLE 2 (Continued)

no.	reaction	A (cm^3 mol s)	n	E_a (cal/mol)	ref
		C_5H_6 reactions			
54	$C_5H_6 + H \leftrightarrow C_2H_2 + C_3H_5$	7.14×10^{-34}	15.1	14 617	59, QRRK
55	$C_5H_6 + H \leftrightarrow C_5H_5 + H_2$	1.20×10^{5}	2.5	1 492	59
56	$C_5H_6 + O \leftrightarrow C_5H_5O_{1-2} + H$	1.00×10^{15}	−0.6	3 669	59, QRRK
57	$C_5H_6 + O \leftrightarrow C_5H_5 + OH$	4.77×10^{4}	2.7	1 106	59
58	$C_5H_6 + OH \leftrightarrow C{=}CC{\cdot}C{=}COH$	4.40×10^{10}	0.82	2 914	59, QRRK
59	$C_5H_6 + OH \leftrightarrow C_5H_5 + H_2O$	3.10×10^{6}	2.0	0	59
60	$C_5H_6 + O_2 \leftrightarrow C_5H_5 + HO_2$	4.00×10^{13}	0.	37 150	59
61	$C_5H_6 + HO_2 \leftrightarrow C_5H_5 + H_2O_2$	1.10×10^{4}	2.6	12 900	59
62	$C_5H_6 + HCO \leftrightarrow C_5H_5 + CH_2O$	1.10×10^{8}	1.9	16 000	59
63	$C_5H_6 + CH_3 \leftrightarrow C_5H_5 + CH_4$	0.18	4.0	0	59
64	$C_5H_6 + C_2H_3 \leftrightarrow C_5H_5 + C_2H_4$	0.12	4.0	0	59
65	$C_5H_6 + C_3H_5 \leftrightarrow C_5H_5 + C_3H_6$	0.20	4.0	0	59
66	$C_5H_6 + CH_2CH\ CHCH \leftrightarrow C_5H_5 + C_4H_6$	0.12	4.0	0	59
67	$C_5H_6 + C_6H_5 \leftrightarrow C_5H_5 + C_6H_6$	0.10	4.0	0	59
68	$C_5H_6 + CH_2CHCCH_2 \leftrightarrow C_5H_5 + C_4H_6$	6.00×10^{12}	0.	0	29 (unchanged)
		C_5H_5 reactions			
69	$C_5H_5 + H \leftrightarrow C_5H_6$	3.20×10^{14}	0.0	0	60, (k_∞)
70	$C_5H_5 + O \leftrightarrow C_5H_5O$	5.20×10^{30}	−5.96	3 445	60, QRRK
71	$C_5H_5 + O \leftrightarrow C_5H_4O + H$	4.25×10^{15}	−0.56	1 230	60, QRRK
72	$C_5H_5 + O \leftrightarrow CH_2CHCHCH + CO$	1.45×10^{1}	3.76	2 213	60, QRRK
73.	$C_5H_5 + OH \leftrightarrow C_5H_4OH + H$	3.63×10^{-48}	18.18	−3 853	60, QRRK
74	$C_5H_5 + HO_2 \leftrightarrow C_5H_5O + OH$	6.19×10^{-31}	13.81	−4 130	60, QRRK
75	$C_5H_5 + HO_2 \leftrightarrow C_5H_4O + H_2O$	9.46×10^{-32}	13.13	−4 803	60, QRRK
76	$C_5H_5 + O_2 \leftrightarrow COC{=}CKET + H$	4.35×10^{7}	1.08	16 737	60, QRRK
77	$C_5H_5 + O_2 \leftrightarrow C{=}CC{=}C{=}O + HCO$	1.31×10^{-3}	4.41	16 472	60, QRRK
		C_4 reactions			
78	$CH_2CHCCH_2 + O_2 \leftrightarrow C_4H_4 + HO_2$	1.20×10^{11}	0.	0	29 (unchanged)
79	$C_4H_4 + OH \leftrightarrow H_2CCCCH + H_2O$	7.50×10^{6}	2.0	5 000	75 (unchanged)
		C_2 reactions			
80	$C_2H_3 + O_2 \leftrightarrow CH_2O + HCO$	4.00×10^{12}	0.	−250	75 (unchanged)
81	$C_2H_2 + H \leftrightarrow C_2H_3$	7.85×10^{14}	−0.22	1 770	QRRK
		C_1 reactions			
82	$CH_2O + OH \leftrightarrow HCO + H_2O$	3.43×10^{15}	1.18	−447	75 (unchanged)
83	$HCO + M \leftrightarrow H + CO + M$	2.50×10^{14}	0.	16 802	75 (unchanged)
84	$CO + O \leftrightarrow CO_2$	1.80×10^{10}	0.	2 438	49, 55 (k_∞)
85	$CO + OH \leftrightarrow CO_2 + H$	3.09×10^{11}	0.	735	76 (unchanged)

[a] Hippler et al.[77] fit to single exponential for temperatures around 800 K. [b] Estimated from $C_6H_5O + H \leftrightarrow C_6H_5OH$.[69] [c] Rate coefficient assumed to have a preexponential factor for diffusion controlled reactions ($A = 10^{12}$ cm^3 mol^{-1} s^{-1}) and no energy barrier ($E_a = 0$). [d] Estimated from the reaction of poly(peroxystyrl)peroxyl radical with phenol using the measurement of $k = 10^7$ cm^3 mol^{-1} $s{-}1$ at 65 °C [78] and assumed $A = 10^{11.5}$ to infer E_a. [e] Estimated from $HO_2 + HO_2 \leftrightarrow H_2O_2 + O_2$.[42] [f] Treated as adjustable parameters.

papers. The reactions between C_5H_5 and C_5H_6 with O_2 and the radical species with the highest rate coefficients at 813 K and 246 bar are included in the SCW benzene oxidation mechanism (R54−R67 and R69−R77). The rates of the H abstraction reactions of C_5H_6 by H, O, OH, HO_2, and O_2 given by Zhong and Bozzelli[59] are generally faster than the predicted rates of the addition/elimination pathways. Resonantly stabilized C_5H_5, instead, reacts exclusively via combination or addition/elimination pathways.

Comparison of Model Predictions to Benzene SCWO Data

The solid line in Figure 2 represents the best possible fit between the predicted and experimental benzene concentration profile using the mechanism in Table 2 with the rate coefficients of the dissociation reactions of C_6H_5OO to $C_6H_4O_2$ and H (R32) and C_5H_5 and CO_2 (R33) treated as adjustable parameters. The reverse rate coefficients of R32 and R33 were calculated by microscopic reversibility using thermochemical data in Table 1. For reference, the predicted profiles from Figure 1 are also shown (long-dashed line). Both the length of the induction time and the shape of the predicted benzene concentration profile agree very well with the experimental data with the inclusion of R32 and R33. The absolute values of the rate coefficients were found not to cause significant differences in the model predictions as long as the rate coefficient of R33 was 40% of that of R32. If $k_{f,33}$ is larger than 40% of $k_{f,32}$, the model predicts too slow a reaction rate of benzene and vice versa. Without inclusion of R32 or R33, the mechanism overpredicts the benzene oxidation rate and the reaction delay is too small (short-dashed line). The dashed-and-dotted line represents the slowest benzene oxidation rate that can be achieved through adjustment of $k_{f,32}$ (without including R33).

As seen in Figure 3, the predicted phenol concentration is in agreement with the experimental measurements with the inclusion of R32 alone or both R32 and R33 in the mechanism. Reaction R32 provides an alternate to R27 for C_6H_5OO consumption, thereby preventing excess C_6H_5O formation. All reactions which lead to phenol formation involve C_6H_5O with the exception of R11. Given that R11 is not competitive with R12 at these conditions, as is discussed shortly, the fact that the experimental and predicted phenol concentrations are in agreement indicates that the C_6H_5O concentration is now properly predicted assuming the C_6H_5O/C_6H_5OH chemistry is correctly represented in the model.

Figure 4 shows the CO and CO_2 concentration predictions after incorporating R32 but without R33. Both CO and CO_2 are underpredicted by the model by up to 2 orders of magnitude.

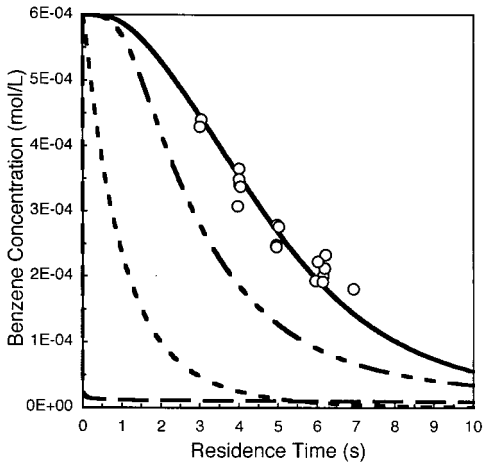

Figure 2. Effect of modifications to the low-pressure benzene oxidation mechanism on predicted benzene concentration: $T = 813$ K; $P = 246$ bar; $\Phi = 1.0$; $[C_6H_6]_0 = 0.6 \times 10^{-3}$ mol/L. Symbols: (○) experimental data; (− −) from Figure 1; (—) mechanism in Table 2 including R32 $C_6H_5OO \leftrightarrow C_6H_4O_2 + H$ with $k_{f,32} = 4.0 \times 10^8$ s^{-1} and R33 $C_6H_5OO \leftrightarrow C_5H_5 + CO_2$ with $k_{f,33} = 1.6 \times 10^8$ s^{-1}; (--) mechanism in Table 2 without R32 or R33; (− -- −) mechanism in Table 2 including only R32 with $k_{f,32} = 4.0 \times 10^8$ s^{-1}.

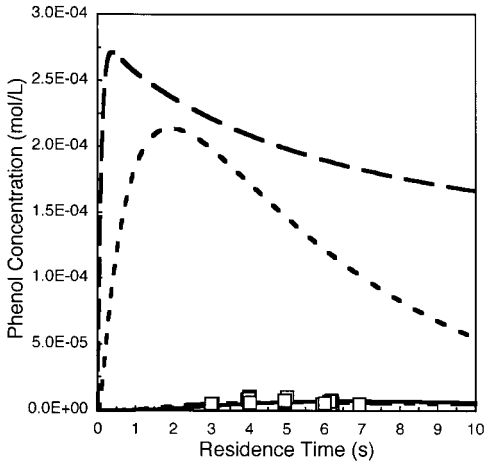

Figure 3. Effect of modifications to the low-pressure benzene oxidation mechanism on predicted benzene concentration: $T = 813$ K; $P = 246$ bar; $\Phi = 1.0$; $[C_6H_6]_0 = 0.6 \times 10^{-3}$ mol/L. Symbols: (○) experimental data; (− −) from Figure 1; (—) mechanism in Table 2 including R32 $C_6H_5OO \leftrightarrow C_6H_4O_2 + H$ with $k_{f,32} = 4.0 \times 10^8$ s^{-1} and R33 $C_6H_5OO \leftrightarrow C_5H_5 + CO_2$ with $k_{f,33} = 1.6 \times 10^8$ s^{-1}; (--) mechanism in Table 2 without R32 or R33; (− -- −) mechanism in Table 2 including only R32 with $k_{f,32} = 4.0 \times 10^8$ s^{-1}.

More importantly, the model predicts that the CO_2 concentration remains below that of CO, while the data clearly show that the opposite is true for all measured residence times. By including R33 in the mechanism (Figure 5), the model properly predicts the CO_2 concentration to exceed that of CO. The model still underpredicts CO and CO_2 concentrations due to a lack of adequate reactions to describe the complete oxidation of all intermediates to CO and CO_2. A large fraction of the carbon remains as $C_6H_4O_2$, and $C_6H_3O_2$, C_5H_5O, C_4H_4, and H_2CCCCH are also significant.

The rate coefficients given here for R32 and R33 are semiempirical and were chosen to improve the fit between the model predictions and the experimental SCWO data. Thus, the rate coefficients for R32 and R33 are specific to this mechanism, and any attempt to use them in other models should be pursued with caution. Reaction R32 was included to account for the

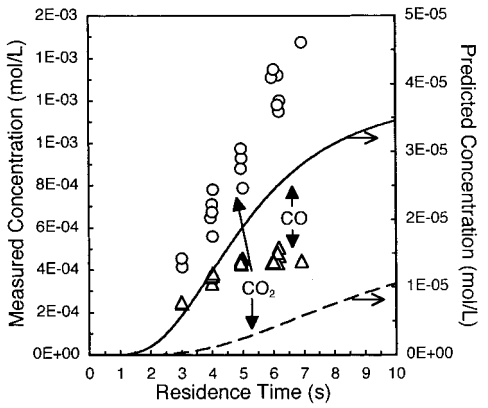

Figure 4. Comparison of predicted (lines, right axis) and experimental (symbols, left axis) CO (△, −) and CO_2 (○, --) concentrations after insertion of $C_6H_5OO \leftrightarrow C_6H_4O_2 + H$ (R32) with $k_{f,32} = 4 \times 10^8$ s^{-1}: $T = 813$ K; $P = 246$ bar; $\Phi = 1.0$; $[C_6H_6]_0 = 0.6 \times 10^{-3}$ mol/L.

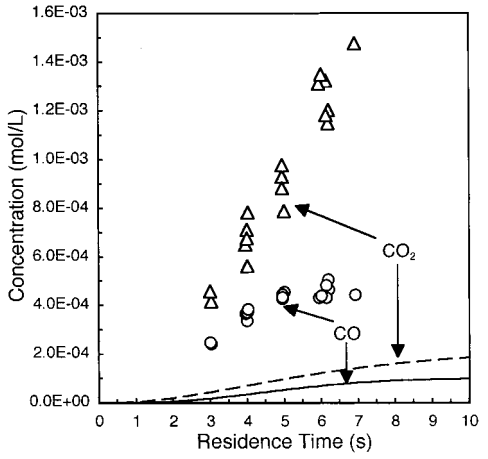

Figure 5. Comparison of predicted (lines) and experimental (symbols) CO (△, −) and CO_2 (○, --) concentrations after insertion of $C_6H_5OO \leftrightarrow C_6H_4O_2 + H$ (R32) with $k_{f,32} = 4 \times 10^8$ s^{-1} and $C_6H_5OO \leftrightarrow C_5H_5 + CO_2$ (R33) with $k_{f,33} = 1.6 \times 10^8$ s^{-1}: $T = 813$ K; $P = 246$ bar; $\Phi = 1.0$; $[C_6H_6]_0 = 0.6 \times 10^{-3}$ mol/L.

observation of $C_6H_4O_2$ in the SCWO of benzene[23] and to be consistent with the incorporation of the overall reaction of C_6H_5 and O_2 to $C_6H_4O_2$ and H in the benzene mechanism of Tan and Frank.[36] Since the reaction between C_6H_5 and O_2 predominantly forms C_6H_5OO at 246 bar and 813 K, R32 was used in place of this addition/elimination reaction. $C_6H_4O_2$ has also been detected during benzene combustion at both fuel-rich and fuel-lean conditions at similar temperatures (900−1300 K).[39] The dissociation reaction of C_6H_5OO to CO_2 and C_5H_5 (R33) was included in order to account for early CO_2 formation. Several other observations of prompt CO_2 formation appear in both the SCWO and the combustion literature. Chai and Pfefferle[39] measured high amounts of CO_2 at low benzene conversions during their study of benzene combustion between 900 and 1300 K and postulated CO_2 production by routes other than the reaction of OH and CO. Savage et al. observed CO_2 yields that always exceeded those of CO in their SCWO studies of phenol[22] and substituted phenols,[61−64] and they too speculated about pathways for CO_2 formation which do not involve CO. In an independent study Krajnc and Levec[65] also reported CO_2 yields which always exceeded those of CO during phenol SCWO, even at the lowest phenol conversions.

Our theoretical calculations using density functional analysis show that all final products used here from the reaction of C_6H_5 and O_2 (C_6H_5O, $C_6H_4O_2$, and C_5H_5) involve one common

isomerization path through a dioxetane cyclic intermediate. After this first isomerization, a path to $C_6H_4O_2 + H$ is present through a ring-opening intermediate. A second series (unzipping process) is also present along with another isomerization series. The rate controlling step to CO_2 involves a 3,2,0 bicyclic (four plus five member ring) tight transition state.[57,66,67] CO_2 results from the unimolecular decomposition of this bicyclic.

Discussion of the Model

The net rates of formation or destruction of key species by the individual reactions in the SCW benzene oxidation mechanism were calculated to determine the controlling reactions at 813 K and 246 bar with stoichiometric oxygen. By comparing the net rates of all reactions involving a single species, the primary destruction and formation pathways were determined.

Benzene was found to react almost exclusively by R11 and R12

$$C_6H_6 + OH \leftrightarrow C_6H_5OH + H \quad (R11)$$

$$C_6H_6 + OH \leftrightarrow C_6H_5 + H_2O \quad (R12)$$

with R12 accounting for over 97% of the oxidation rate of benzene at 813 K and 246 bar. Although R11 is recognized to proceed by a chemically activated pathway,[68] given the relative unimportance of R11 the rate coefficient used here is the same as that used by Shandross.[69] Phenol is initially formed by R11, destroyed by R18, and then re-formed by R21 in an equimolar exchange:

$$C_6H_5OH + CH_2CHCHCH \leftrightarrow C_6H_5O + C_4H_6 \quad (R18)$$

$$C_6H_5O + C_5H_6 \leftrightarrow C_6H_5OH + C_5H_5 \quad (R21)$$

Given that R18 and R21 are the principal reactions involving both C_6H_5O and C_6H_5OH and that C_6H_5OH is minor compared to C_6H_5 as a benzene decomposition product, C_6H_5O is also not a key intermediate in the SCW benzene oxidation mechanism. Phenyl radical (C_6H_5) formed by R12 reacts completely through R26:

$$C_6H_5 + O_2 \leftrightarrow C_6H_5OO \quad (R26)$$

The fate of C_6H_5OO is the most critical unknown. Comparisons with the data suggest that the radical-forming, chain-branching loss channel to C_6H_5O and O (R27) can only be a minor channel. Under SCWO conditions, most C_6H_5OO appears to decay via the two thermal pathways:

$$C_6H_5OO \leftrightarrow C_6H_4O_2 + H \quad (R32)$$

$$C_6H_5OO \leftrightarrow C_5H_5 + CO_2 \quad (R33)$$

p-Benzoquinone formed by R32 undergoes oxidation as described by the mechanism of Alzueta et al.[58] while C_5H_5 formed by R33 reacts primarily by R74:

$$C_5H_5 + HO_2 \leftrightarrow C_5H_5O + OH \quad (R74)$$

C_5H_5O then undergoes ring opening reactions leading eventually to CO and CO_2.

Since the oxidation of benzene proceeds mainly by the H-abstraction channel (R12), the reaction delay (or induction time) and subsequent rate of benzene reaction is determined by the rate of OH radical generation which, in the present mechanism, is primarily by R74.

If R32 and R33 are not incorporated into the mechanism, R27 is the dominant C_6H_5OO destruction channel:

$$C_6H_5OO \leftrightarrow C_6H_5O + O \quad (R27)$$

With O formed by R27, excess OH is generated directly by −R7

$$O + H_2O \leftrightarrow OH + OH \quad (-R7)$$

and indirectly by the following series of reactions:

$$C_6H_6 + O \leftrightarrow C_6H_5O + H \quad (R13)$$

$$H + O_2 \leftrightarrow HO_2 \quad (R1)$$

$$HO_2 + HO_2 \leftrightarrow H_2O_2 + O_2 \quad (R2)$$

$$H_2O_2 \leftrightarrow OH + OH \quad (-R4)$$

R12 proceeds too quickly, and the present mechanism overpredicts the benzene oxidation rate.

Including R32 with a higher rate constant than R27 eliminates the rapid formation of O and the subsequent overproduction of OH by −R7. Since R32 generates H, OH formation proceeds through R1, R2, and −R4, and R32 alone cannot decrease the benzene oxidation rate sufficiently to bring the model into agreement with the data. Including R33 slows the benzene oxidation rate, since C_5H_5 is relatively unreactive, while providing a pathway for CO_2 formation, thus accounting for the experimental observation that CO_2 yields exceed those of CO for all measured residence times and reaction conditions.[23]

Model-Data Comparison at Other Conditions

The solid line in Figure 2 represents the best possible fit of the model to the experimental benzene concentration profile at 813 K and 246 bar and with stoichiometric oxygen using the mechanism in Table 2 with the rate coefficients for the dissociation of C_6H_5OO to $C_6H_4O_2$ and H (R32) and to C_5H_5 and CO_2 (R33) treated as adjustable parameters. As a test of the robustness of the mechanism, the model predictions were compared to experimental benzene SCWO data measured at varying reactor conditions.[23] No further adjustments were made to the mechanism to improve model−data agreement in performing this comparison. The rate coefficients of R32 and R33 were treated as temperature independent and maintained at their values given in Table 2.

Temperature Variations. Figure 6 shows a comparison of the model predictions to experimental benzene conversion data measured as a function of temperature at 246 bar with stoichiometric oxygen and a residence time of 6.2 s. The model and data are in excellent agreement across the entire temperature range.

Fuel Equivalence Ratio Variations. In Figure 7 the predicted benzene concentration profiles are compared to the experimental data measured at 813 K and 246 bar as a function of residence time with fuel equivalence ratios (Φ) of 0.5 (100% excess oxygen), 1.0 (stoichiometric oxygen), and 2.5 (40% of oxygen demand). The experimental and predicted residence times profiles at $\Phi = 1.0$ are those from Figure 2. The model qualitatively captures the trend of benzene conversion, increasing with the increasing oxygen concentration, and quantitatively agrees with the data measured at fuel-lean conditions. The experimental data for the fuel-rich conditions appear to exhibit a more moderate oxidation rate than the model predicts.

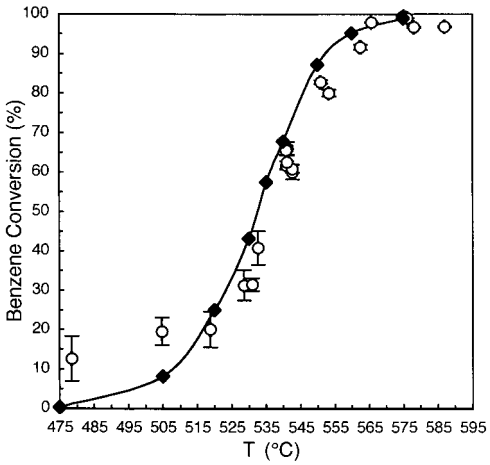

Figure 6. Comparison of predicted (−◆−) and measured (○) benzene conversions at various temperatures: $\tau = 6.2$ s; $P = 246$ bar; $\Phi = 1.0$; $[C_6H_6]_0 = 0.6 \times 10^{-3}$ mol/L.

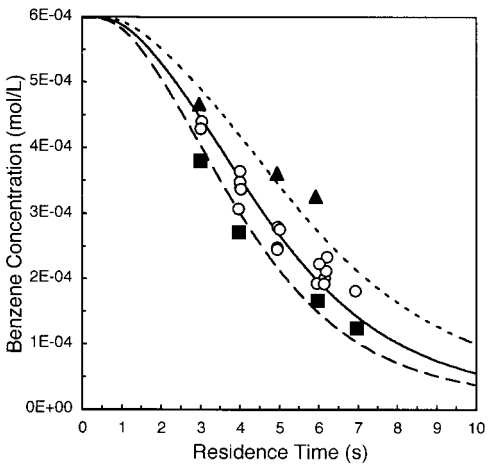

Figure 7. Comparison of predicted (lines) and measured (symbols) benzene concentrations at three fuel equivalence ratios (Φ) (■, − −) $\Phi = 0.5$, (○, −) $\Phi = 1.0$, and (▲, --) $\Phi = 2.5$: $T = 813$ K; $P = 246$ bar; $[C_6H_6]_0 = 0.6 \times 10^{-3}$ mol/L.

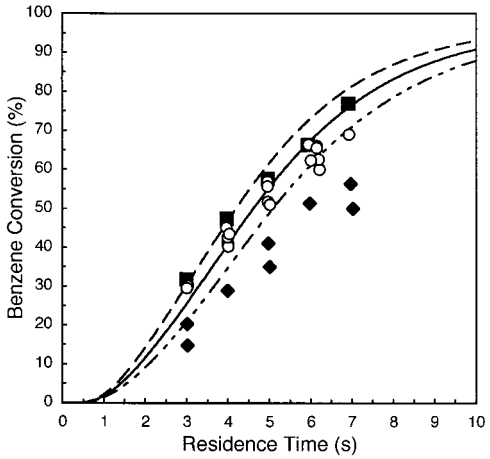

Figure 8. Comparison of predicted (lines) and measured (symbols) benzene conversions at three different initial benzene concentrations (■, − −) $[C_6H_6]_0 = 0.4$ mM, (○, −) $[C_6H_6]_0 = 0.6$ mM, and (◆, − -- −) $[C_6H_6]_0 = 1.2$ mM: $T = 813$ K; $P = 246$ bar; $\Phi = 1.0$.

Benzene Concentration Variations. Figure 8 compares the predicted and experimental conversions with initial benzene concentrations of 0.4, 0.6, and 1.2 mM. The predicted benzene conversion profile and experimental data with $[C_6H_6]_0 = 0.6$ mM are those from Figure 2. The model does qualitatively reproduce the trend of decreasing conversion with increasing initial benzene concentration, but the quantitative agreement, especially with that of the 1.2 mM data, is poor.

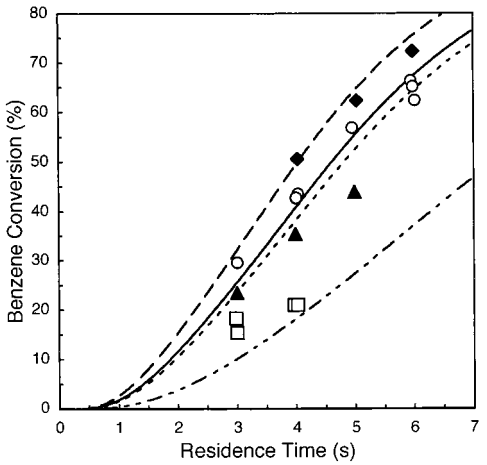

Figure 9. Comparison of predicted (lines) and measured (symbols) benzene conversions at four water densities (◆, − −) $\rho = 0.091$ g/mL ($P = 278$ bar), (○, −) $\rho = 0.079$ g/mL ($P = 246$ bar), (▲, --) $\rho = 0.072$ g/mL ($P = 228$ bar), and (□, − -- −) $\rho = 0.041$ g/mL ($P = 139$ bar): $T = 813$ K; $[C_6H_6]_0 = 0.6 \times 10^{-3}$ mol/L; $\Phi = 1.0$.

Density Variations. As a final test, Figure 9 compares the predicted benzene conversion with experimental data at four water densities: 0.041, 0.072, 0.079, and 0.091 g/mL. The predicted benzene conversion profile and experimental data at 0.079 g/mL ($P = 246$ bar) are those from Figure 2. The model both qualitatively captures the experimentally observed trend of benzene conversion by SCWO increasing with the increasing water concentration and gives excellent quantitative agreement.

Summary and Conclusions

Supercritical water (SCW) benzene oxidation data were modeled using an available low-pressure, gas-phase benzene combustion mechanism and submechanisms describing the oxidation of key intermediate species in benzene oxidation. The important modifications necessary to adapt the benzene combustion mechanism to the lower temperatures and higher pressures of SCWO were as follows: (1) the adaptation of the following unimolecular and bimolecular recombination reactions for pressure

$$H + O_2 \leftrightarrow HO_2 \quad \text{(R1)}$$

$$OH + OH \leftrightarrow H_2O_2 \quad \text{(R4)}$$

$$H + O_2 \leftrightarrow OH + O \quad \text{(R6)}$$

$$C_2H_2 + H \leftrightarrow C_2H_3 \quad \text{(R81)}$$

$$CO + O \leftrightarrow CO_2 \quad \text{(R84)}$$

(2) the inclusion of a pressure-corrected C_5H_5/C_5H_6 submechanism; (3) use of the reaction pathways and rate coefficients predicted by CHEMDIS for

$$C_6H_5 + O_2 \leftrightarrow C_6H_5O + O \quad \text{(R25)}$$

$$C_6H_5 + O_2 \leftrightarrow C_6H_5OO \quad \text{(R26)}$$

$$C_6H_5OO \leftrightarrow C_6H_5O + O \quad \text{(R27)}$$

(4) the insertion of bimolecular reactions involving C_6H_5OO;

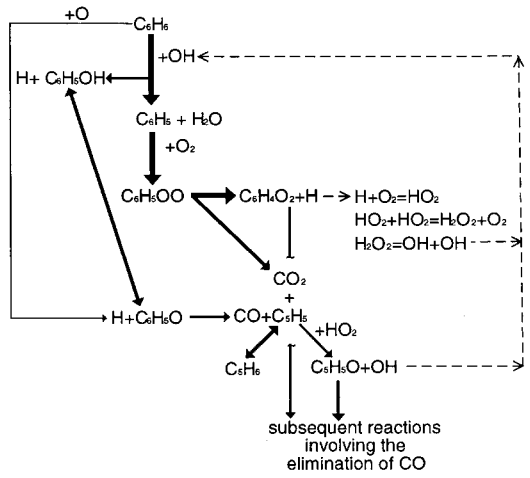

Figure 10. Representation of the major oxidation pathways in the final SCWO benzene combustion mechanism.

and (5) the addition of the thermal dissociation reactions of C_6H_5OO:

$$C_6H_5OO \leftrightarrow C_6H_4O_2 + H \qquad \text{(R32)}$$

$$C_6H_5OO \leftrightarrow C_5H_5 + CO_2 \qquad \text{(R33)}$$

By adjusting the rate coefficients of R32 and R33, the model was fit to the benzene concentration profile measured in the benzene supercritical water oxidation (SCWO) experiments at 813 K and 246 bar with stoichiometric oxygen. Using the resulting mechanism, the main pathways of which are depicted in Figure 10, both the benzene and phenol concentration profiles were accurately predicted. Carbon monoxide and carbon dioxide were both severely underpredicted, but the model did correctly predict the concentration of CO_2 to exceed that of CO at all residence times. The disagreement between the predicted and experimentally measured CO and CO_2 concentrations is due to inadequate chemistry for the further oxidation of the linear C_6, C_5, C_4 intermediate species to CO and CO_2. A comparison of the model predictions to benzene SCWO data measured at conditions other than those to which the model was fit revealed that the model qualitatively explains the trends of the data and gives good quantitative agreement at many conditions. For example, the model predicts the measured benzene conversion to better than $\pm$10% conversion at temperatures between 790 and 860 K (515 and 590 °C) at 246 bar with stoichiometric oxygen and at pressures from 139 to 278 bar at 813 K with stoichiometric oxygen.

The most important difference between this benzene SCWO mechanism and those previously developed for combustion conditions is the inclusion of reactions involving C_6H_5OO predicted to be formed from the reaction between C_6H_5 and O_2. Mechanisms developed for combustion conditions have set the products of this reaction equal to C_6H_5O and O and/or C_2H_2, C_2H_3, and CO through a semiglobal pathway. Of the reactions included to account for the destruction of C_6H_5OO, the two thermal decomposition pathways to $C_6H_4O_2$ and H (R32) and C_5H_5 and CO_2 (R33) were most important. Without their inclusion, the predicted oxidation rate of benzene was too fast and the concentration of CO was incorrectly predicted to exceed that of CO_2. Although the rate coefficients for these two reactions were treated as adjustable parameters and should not be used in mechanisms developed for different conditions, the inclusion of these pathways is justified given the experimental observation of $C_6H_4O_2$ at similar conditions and the apparent need for reactions which will form CO_2 early in the oxidation process. The good agreement achieved between the model predictions and the experimental SCWO data may be fortuitous, but the fact that the model both qualitatively and quantitatively reproduced the experimental data is encouraging given that the data were gathered at very different temperature, pressure (density), and oxygen concentration conditions than those for which the original benzene combustion mechanism was developed.

Acknowledgment. The authors gratefully acknowledge K. A. Smith, W. A. Peters, the other members of the MIT SCWO research group, R. A. Shandross, H. Richter, and D. F. Kronholm for assistance with the research documented within this publication. Partial support for this research was provided by the Army Research Office through its University Research Initiative (Grant No. DAAL03-92-G-0177) and AASERT Programs (Grant No. DAAH04-94-G-0145), both under the supervision of Robert Shaw, by Sandia National Laboratories through its Strategic Environmental Research and Development Program (SERDP) under the direction of Steven Rice, and by the National Institute of Environmental Health Sciences (NIEHS) Superfund program.

Supporting Information Available: Tables IS−VS, listing data used in the QRRK analysis of the rate coefficients of R1, R4, R6, R25, R26, R27, R81, and R84 in Table 2 by CHEMDIS or CHEMACT, are available free of charge via the Internet at http://pubs.acs.org.

References and Notes

(1) Killilea, W. R.; Swallow, K. C. *J. Supercrit. Fluids* **1992**, *5*, 72.
(2) Modell, M. *Supercritical water oxidation*; Freeman, H. M., Ed.; McGraw-Hill: New York, 1989; p 8.153.
(3) Tester, J. W.; Holgate, H. R.; Armellini, F. J.; Webley, P. A.; Killilea, W. E.; Hong, G. T.; Barner, H. E. *ACS Symp. Ser.* **1993**, *518*, Chapter 3.
(4) Gloyna, E. F.; Li, L. *Environ. Prog.* **1995**, *14*, 182.
(5) Tester, J. W.; Cline, J. A. *Corrosion* **1999**, *55*, 1088.
(6) Holgate, H. R.; Tester, J. W. *Combust. Sci. Technol.* **1993**, *88*, 369.
(7) Dagaut, P.; Daney de Marcillac, B.; Tan, Y.; Cathonnet, M.; Boettner, J.-C. *J. Chim. Phys.* **1995**, *92*, 1124.
(8) Brock, E. E.; Savage, P. E. *AIChE J.* **1995**, *41*, 1874.
(9) Dagaut, P.; Cathonnet, M.; Boettner, J.-C. *J. Supercrit. Fluids* **1996**, *9*, 33.
(10) Lamb, W. J.; Hoffman, G. A.; Jonas, J. *J. Chem. Phys.* **1981**, *74*, 6875.
(11) Uematsu, M.; Frank, E. U. *J. Phys. Chem. Ref. Data* **1980**, *9*, 1291.
(12) Marshall, W. L.; Franck, E. U. *J. Phys. Chem. Ref. Data* **1981**, *10*, 295.
(13) Holgate, H. R.; Tester, J. W. *J. Phys. Chem.* **1994**, *98*, 810.
(14) Paterson, C.; Breshears, D.; Foy, B. *Combust. Sci. Technol.* **1993**, *89*.
(15) Alkam, M. K.; Pai, V. M.; Butler, P. B.; Pitz, W. J. *Combust. Flame* **1996**, *106*, 110.
(16) Webley, P. A.; Tester, J. W. *Energy Fuels* **1991**, *5*, 411.
(17) Savage, P. E.; Yu, J. L.; Stylski, N.; Brock, E. E. *J. Supercrit. Fluids* **1998**, *12*, 141.
(18) Schmitt, R. G.; Butler, P. B.; Westbrook, C. K.; Pitz, W. J. U.S. Department of Energy DE92-008559, 1991.
(19) Butler, P. B.; Bergan, N. E.; Bramlette, T. T.; Westbrook, C. K.; Pitz, W. J. U.S. Department of Energy DE92-008565, 1991.
(20) Webley, P. A.; Tester, J. W. *ACS Symp. Ser.* **1989**, *406*, 259.
(21) Butler, P. B.; Bergan, N. E.; Bramlette, T. T.; Pitz, W. J.; Westbrook, C. K. U.S. Department of Energy DE91-017097, 1991.
(22) Gopalan, S.; Savage, P. E. *ACS Symp. Ser.* **1995**, *608*, 217.
(23) DiNaro, J. L.; Tester, J. W.; Swallow, K. C.; Howard, J. B. *AIChE J.*, in press.
(24) DiNaro, J. L.; Howard, J. B.; Green, W. H.; Tester, J. W.; Bozzelli, J. W. *28th (Int.) Symp. Combust.*, in press.
(25) Brezinsky, K. *Prog. Energy Combust. Sci.* **1986**, *12*, 1.
(26) Bittker, D. A. *Combust. Sci. Technol.* **1991**, *79*, 49.
(27) Lovell, A. B.; Brezinsky, K.; Glassman, I. *22nd Symp. (Int.) Combust.* **1988**, 1063.
(28) Burcat, A.; Snyder, C.; Brabbs, T. NASA TM-87312, 1986.

(29) Emdee, J. L.; Brezinsky, K.; Glassman, I. *J. Phys. Chem.* **1992**, *96*, 2151.
(30) Lindstedt, R. P.; Skevis, G. *Combust. Flame* **1994**, *99*, 551.
(31) Bittner, J. D.; Howard, J. B. *18th Symp. (Int.) Combust.* **1980**, 1105.
(32) Zhang, H.-Y.; McKinnon, J. T. *Combust. Sci. Technol.* **1995**, *107*, 261.
(33) Robinson, P. J.; Holbrook, K. A. *Unimolecular Reactions*; Wiley-Interscience: London, 1972.
(34) Shandross, R. A.; Longwell, J. P.; Howard, J. B. *26th Symp. (Int.) Combust.* **1996**, 711.
(35) Shandross, R. A. Experimental and theoretical study of hydrogen and benzene destruction chemistries. Ph.D. Thesis, Massachusetts Institute of Technology, 1996.
(36) Tan, Y.; Frank, P. *26th Symp. (Int.) Combust.* **1996**, 677.
(37) Tan, Y.; Dagaut, P.; Cathonnet, M.; Boettner, J.-C. *Combust. Sci. Technol.* **1994**, *102*, 21.
(38) Frank, P.; Herzler, J.; Just, T.; Wahl, C. *25th Symp. (Int.) Combust.* 1994.
(39) Chai, Y.; Pfefferle, L. D. *Fuel* **1998**, *77*, 313.
(40) Kronholm, D. F. Molecular weight growth pathways in fuel rich combustion. Ph.D. Thesis, Massachusetts Institute of Technology, 2000.
(41) Lutz, A. E.; Kee, R. J.; Miller, J. A. Sandia National Laboratories SAND87-8248, 1988.
(42) Baulch, D. L.; Cobos, C. J.; Cox, R. A.; Esser, C.; Frank, P.; Just, T.; Kerr, J. A.; Pilling, M. J.; Troe, J.; Walker, R. W.; Warnatz, J. *J. Phys. Chem. Ref. Data* **1992**, *21*, 411.
(43) Madronich, S.; Felder, W. *J. Phys. Chem.* **1985**, *89*, 3556.
(44) Baulch, D. L.; Cobos, C. J.; Cox, R. A.; Frank, P.; Hayman, G.; Just, T.; Kerr, J. A.; Murrells, T.; Pilling, M. J.; Troe, J.; Walker, R. W.; Warnatz, J. *J. Phys. Chem. Ref. Data* **1994**, *23*, 847.
(45) Dean, A. M. *J. Phys. Chem.* **1985**, *89*, 4600.
(46) Dean, A. M.; Bozzelli, J. W.; Ritter, E. R. *Combust. Sci. Technol.* **1991**, *80*, 63.
(47) Ing, W.-C. Reaction Kinetics of Methanol and MTBE: Oxidation and Pyrolysis. Ph.D. Thesis, New Jersey Institute of Technology, **1995**.
(48) Chang, A. Y.; Bozzelli, J. W.; Dean, A. M. *Z. Phys. Chem.*, in press.
(49) Westmoreland, P. R.; Howard, J. B.; Longwell, J. P.; Dean, A. M. *AIChE J.* **1986**, *32*, 1971.
(50) Cobos, C. J.; Hippler, H.; Troe, J. *J. Phys. Chem.* **1985**, *89*, 342.
(51) Fulle, D.; Hamann, H. F.; Hippler, H.; Troe, J. *J. Chem. Phys.* **1996**, *105*, 1001.
(52) Forster, R.; Frost, M.; Fulle, D.; Hamann, H. F.; Hippler, H.; Schlepegrell, A.; Troe, J. *J. Chem. Phys.* **1995**, *103*, 2949.
(53) Kim, T. J.; Yetter, R. A.; Dryer, F. L. *25th Symp. (Int.) Combust.* **1994**, 759.
(54) Warnatz, J. In *Rate coefficients in the C/H/O system*; Gardiner, W. C., Ed.; Springer-Verlag: New York, 1984; p 197.
(55) Troe, J. *15th Symp. (Int.) Combust.* **1974**, 667.
(56) Yu, T.; Lin, M. C. *J. Am. Chem. Soc.* **1994**, *116*, 9571.
(57) Carpenter, B. K. *J. Am. Chem. Soc.* **1993**, *115*, 9806.
(58) Alzueta, M. U.; Oliva, M.; Glarborg, P. *Int. J. Chem. Kinet.* **1998**, *30*, 683.
(59) Zhong, X.; Bozzelli, J. W. *Int. J. Chem. Kinet.* **1997**, *29*, 893.
(60) Zhong, X.; Bozzelli, J. W. *J. Phys. Chem.* **1998**, *102*, 3537.
(61) Martino, C. J.; Savage, P. E.; Kasiborski, J. *Ind. Eng. Chem. Res.* **1995**, *34*, 1941.
(62) Martino, C. J.; Savage, P. E. *Ind. Eng. Chem. Res.* **1997**, *36*, 1391.
(63) Martino, C. J.; Savage, P. E. *Ind. Eng. Chem. Res.* **1999**, *38*, 1784.
(64) Martino, C. J.; Savage, P. E. *Ind. Eng. Chem. Res.* **1999**, *38*, 1775.
(65) Krajnc, M.; Levec, J. *AIChE J.* **1996**, *42*, 1977.
(66) Bozzelli, J. W. Unpublished work.
(67) Barckholtz, C.; Fadden, M. F.; Hadad, C. M. *J. Phys. Chem.* **1999**, *103*, 8108.
(68) Lay, T. S.; Bozzelli, J. W.; Seinfeld, J. H. *J. Phys. Chem.* **1996**, *100*, 6543.
(69) He, Y. Z.; Mallard, W. G.; Tsang, W. *J. Phys. Chem.* **1988**, *92*, 2196.
(70) Gardiner, W. C. *Combustion Chemistry*; Springer-Verlag: New York, 1984; p 509.
(71) Burcat, A.; Zeleznik, F. J.; McBride, B. J. NASA Technical Memorandum 83800, 1985.
(72) Kee, R. J.; Rupley, F. M.; Miller, J. A. Sandia National Laboratories SAND87-8215B, 1994.
(73) Burcat, A.; McBride, B. Israel Institute of Technology TAE 732, 1995 and updates.
(74) Ko, T.; Adusei, G. Y.; Fontijn, A. *J. Phys. Chem.* **1991**, *95*, 8745.
(75) Miller, J. A.; Melius, C. F. *Combust. Flame* **1992**, *91*, 21.
(76) Dixon-Lewis, G. *Proc. R. Soc. London A* **1972**, *330*, 219.
(77) Hippler, H.; Troe, J.; Willner, J. *J. Chem. Phys.* **1990**, *93*, 1755.
(78) Howard, J. A.; Ingold, K. U. *Can. J. Chem.* **1963**, *41*, 1744.